Results in Engineering 20 (2023) 101604

Contents lists available at ScienceDirect

Results in Engineering

journal homepage: www.sciencedirect.com/journal/results-in-engineering

Precise forecasting of scour depth downstream of flip bucket spillway through data-driven models

Mehdi Fuladipanah [a,*], H Md Azamathulla [b], Kiran Tota-Maharaj [c], Vishwanadham Mandala [d], Aaron Chadee [e]

[a] Department of Civil Engineering, Ramhormoz Branch, Islamic Azad University, Ramhormoz, Iran
[b] Civil Engineering and Environmental Engineering, The University of the West Indies, St. Augustine Campus, Trinidad
[c] Department of Civil Engineering, School of Infrastructure & Sustainable Engineering, College of Engineering and Physical Sciences, Aston University, Birmingham, Aston Triangle, Birmingham, UK
[d] Enterprise Architect, Indiana University, Bloomington, IN, US.MS in Data Science, IU Bloomington, USA
[e] Civil and Environmental Engineering, University of the West Indies, St Augustine Campus, Trinidad

ARTICLE INFO

Keywords:
Dam safety
Machine learning
Performance assessment
Scour depth forecasting

ABSTRACT

Flip-bucket spillways are utilized in hydraulic engineering to diminish the kinetic energy of flowing water by redirecting the flow jet into the air. In the downstream stailing basin with low tail-water, sediment particles movement results in scour hole formation, posing a threat to spillway stability. The accurate prediction of scour hole depth is a crucial area of the present research work. This study endeavors to employ four data-driven models (DDMs), namely Support Vector Machine (SVM), Gene Expression Programming (GEP), Multilayer Perceptron (MLP), and Multivariate Adaptive Regression Splines (MARS), in combination with five selected empirical equations. The objective is to accurately predict scour depth utilizing field-collected data from site number 84. Relative scour depth, $\frac{d_s}{H_1}$, was simulated based on the readily extracted parameter i.e. Froude number, $Fr = \frac{q}{\sqrt{gH_1^3}}$. The evaluation of model performance was conducted using fundamental metrics, including root mean square error (RMSE), coefficient of determination (R^2), mean average error (MAE), and the maximum value of the developed discrepancy ratio (DDRmax). Among the DDMs, the MARS model demonstrated superior performance in both the training and testing phases. In the training phase, it yielded metrics (RMSE = 0.08665, MAE = 0.05714, R^2 = 0.99169, DDRmax = 4.519), and in the testing phase, it produced metrics (RMSE = 0.0252, MAE = 0.0170, R^2 = 0.09933, DDRmax = 9.144). This exceptional performance of the MARS model surpassed the initially selected (Wu, 1973) [1] experimental model, which exhibited metrics (RMSE = 0.39667, MAE = 0.17463, R^2 = 0.96172, DDR = 1.428). The evaluation indices conclusively establish the MARS method's absolute superiority over the experimental approach proposed by Wu (1973) [1].

1. Introduction

Spillways constitute an essential component of dam structures, serving the critical function of releasing excess floodwater beyond the reservoir's storage capacity, in accordance with established operational protocols [1]. This controlled release is imperative for maintaining the structural integrity of the dam and safeguarding the adjacent environment. As the demand for effective flood energy dissipation solutions at the dam's base has grown, various configurations of bucket-type energy dissipaters have been developed. Economic considerations have increasingly driven designers to employ ski-jump buckets as a preferred waterworks solution for energy dissipation (see Fig. 1).

Trajectory or flip-bucket devices serve as energy dissipators located at the base of spillways in situations where tail-water levels in the stilling basin are inadequate for the formation of a hydraulic jump. The bucket redirects high-velocity flows as a jet, dissipating energy during flight and landing at a safe distance downstream to prevent riverbed damage that could jeopardize the spillway structure. This method is commonly employed in high spillways due to its cost-effectiveness compared to a deep and expensive hydraulic jump-type stilling basin.

* Corresponding author.
E-mail addresses: fuladipanah@gmail.com (M. Fuladipanah), hazi.azamathulla@sta.uwi.edu (H.M. Azamathulla), k.tota-maharaj@aston.ac.uk (K. Tota-Maharaj), Vmandala@iu.edu (V. Mandala), aaron.chadee@hotmail.com (A. Chadee).

https://doi.org/10.1016/j.rineng.2023.101604
Received 29 August 2023; Received in revised form 3 November 2023; Accepted 15 November 2023
Available online 28 November 2023
2590-1230/

It is particularly useful in cases where the hydraulic characteristics of the downstream channel are unstable, making accurate predictions of tailwater depths in the stilling basin challenging [3,4]. When the jet enters the tailwater it has already been partially disintegrated through interaction with the surrounding air. The impact of the plunging jet however is still great 'enough to scour the channel bottom. At the point of impact with the bed material the turbulent eddies of the plunging jet are deflected horizontally downstream creating drag forces on the credible materiel greater than the resisting forces, The scoured material is transported downstream to a point where the resisting forces are greater than the drag forces and a scour hole is gradually formed, As the scour hole deepens the degree of turbulence of the plunging jet decreases until a point of equilibrium is reached between the resisting force of the bed material and the drag force resulting in a dish shaped scour hole being formed [4].

The depth of this scour hole, denoted as d_s in Fig. 1, can be expressed as a function of various factors, including the discharge intensity per unit width (q), the height of fall (H_1), the bucket radius (R), the flip bucket angle (Φ), and the characteristics of the sediment particles such as their size and type [5]. Considerable horizontal distance is traversed by the trajectory originating from the flip-bucket toe before it contacts the riverbed. This distance is contingent upon several parameters, namely the flow discharge, the radius and lip angle of the bucket, and the velocity of the flow as it enters the ski-jump bucket. As a consequence of this trajectory, a scour hole is formed immediately downstream of the point where the jet affects the riverbed. The determination and prediction of scour hole characteristics play a pivotal role in enhancing the safety design and structural stability of both the dam and the spillway. Over the course of several decades, numerous empirical formulas have been developed by researchers to estimate scour depth. Table 1 highlights some of the widely recognized and popular empirical formulas in this regard.

While the above-mentioned formulas offer convenience in practical application, they are not without their limitations. Typically, these formulas describe an idealized, approximate, and average scenario of prototype conditions. Consequently, there often exists a disparity between the estimated values derived from these formulas and the actual, on-site conditions. Due to the constraints imposed by time and cost considerations, physical hydraulic models are primarily employed in research endeavors. An alternative approach employed for simulating ds involves Computational Fluid Dynamic (CFD) modeling. However, this method is characterized by its inherent complexity and the limitations associated with its results, which have been identified as key drawbacks. Moreover, additional limitations further contribute to its disadvantages. Consequently, there has been a growing interest among researchers in the application of soft-computing methods, particularly Artificial Intelligence (AI) to estimate d_s including: the ANN, Adaptive Neuro-Fuzzy Inference System (ANFIS), Genetic Algorithms (GA), Harris hawks optimization (HHO) Bagging Regressor (BR), multivariate adaptive regression splines (MARS), radial basis function (RBF) network, classification and regression tree (CART), Granular Computing (GC), Particle Swarm Optimization (PSO), the SVM, Light Gradient Boosting Machine (LightGBM), Support Vector Regression (SVR), Cascaded Forward Neural Network (CFNN), Kernel Ridge Regression (KRR), Adaptive Boosting Regressor (ABR), Random Forest (RF), Random Tree (RT), Reduces Error Pruning Tree (REP Tree), Gradient Boosting Decision Tree (GBDT), Extreme Gradient Boosting (XGBoost) and the GEP [12–15]. The utilization of MLMs has been suggested by numerous researchers to forecast phenomena such as scour depth. However, the absence of empirically measured or recorded data can be articulated as a limitation or drawback in their application. Table 2 provides a comprehensive literature review detailing the utilization of Data-Driven Models (DDMs) in various applications.

This present paper distinguishes itself from prior research endeavors in a novel manner by employing field data, which accurately mirror the genuine response conditions concerning hydraulic and physical parameters. The preceding studies collectively demonstrate the commendable performance of DDMs in the prediction of scour depth downstream of spillways. The research is further motivated by the adaptability and potential exhibited by DDMs including the SVM, the GEP, multilayer perceptron (MLP) and the MARS in addressing the intricacies of scour phenomena. Additionally, established empirical formulas are integrated to estimate scour depth. To evaluate the efficacy of these empirical equations in comparison to DDMs, several statistical indices are employed for performance assessment.

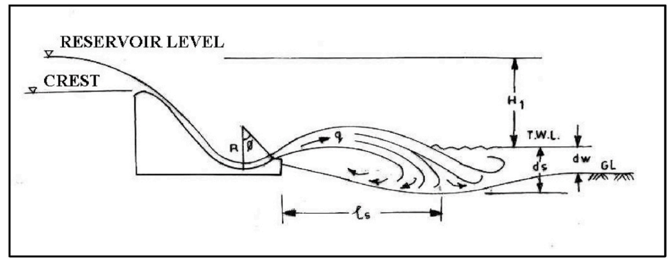

Fig. 1. Scour below flip bucket spillway [2].

2. Methods and materials

2.1. The dataset used

While laboratory models offer several advantages, including the generation of substantial data and the ability to repeat tests, they are not without limitations and drawbacks. Issues such as the scale effect and challenges in accurately replicating the geometric and morphological characteristics of riverbeds and flow conditions underscore the need for caution when relying solely on laboratory models. These limitations make a compelling case for prioritizing the use of field data, despite their relatively limited quantity. Consequently, the decision was made to employ field data for simulating scour depth downstream of the flip bucket spillway. In this study, a total dataset comprising 84 data points was compiled. These data were sourced from various references, including Damel et al. (1966), [1,10,28–32]; the website 'http://www.ferc.gov/industries/hydropower/safety/eng-guide/chap11.pdf', and [33]. Table 3 provides a comprehensive presentation of the compiled measurements. The geometric and hydraulic parameters referenced in this table are visually depicted in Fig. 1. The overall variation of the dependent variable, d_s, concerning the independent variables is visually depicted in Fig. 2.

2.2. Overview of SVM

Introduced and advanced by Ref. [34]; the SVM represents a self-organizing method capable of addressing classification, regression, and pattern recognition challenges. Its algorithm is grounded in the principle of minimizing structural risk during the resolution of intricate problems through a combination of training and testing procedures. The ultimate objective of the SVM is to minimize the disparity between predicted and target datasets by optimizing parameter settings. The mathematical model underlying this optimization process can be elucidated as follows:

$$\text{Minimize}: R_{SVM}(\omega, \xi^*) = \frac{1}{2}\|\omega\|^2 + C\sum_{i=1}^{n}(\xi_i + \xi_i^*) \tag{12}$$

Subject:

$$d_i - \omega\varphi(x_i) + b_i \leq \varepsilon + \xi_i \tag{13}$$

$$\omega\varphi(x_i) + b_i - d_i \leq \varepsilon + \xi_i \tag{14}$$

$$\xi_i, \xi_i^* \geq 0 \quad i = 1, 2, \ldots, l \tag{15}$$

Table 1
A summary literature of the empirical equations to predict d_s D/S of the flip-bucket spillway.

Eq. No.	Reference	Formula	Recommendations
(1)	[6]	$d_s = \frac{3.15q^{0.57}H_1^{0.2}}{d_m^{0.32}}$	d_s: scour hole depth, m q: discharge intensity, m^2/s H_1: fall height, m d_m: sediment mean size, m
(2)	[7]	$d_s = 1.90q^{0.54}H_1^{0.225}$	d_s: scour hole depth, m q: discharge intensity, m^2/s H_1: fall height, m
(3)	[8]	$d_s = A(qH_1)^{0.5}$	ds: scour hole depth, m q: discharge intensity, m^2/s H_1: fall height, m A = 0.65 denotes ultimate maximum scour A = 0.54 represents probable scour under sustained operation A = 0.36 yields minimum expected to scour
(4)	[9]	$d_s = \frac{1.235q^{0.67}H_1^{0.18}}{d_{50}^{0.063}}$	d_s: scour hole depth, ft q: discharge intensity, ft^2/s H_1: fall height, ft d_{50}: sediment mean size, ft
(5)	[1]	$\frac{d_s}{H_1} = 2.11\left(\frac{q}{\sqrt{gH_1^3}}\right)^{0.51}$	d_s: scour hole depth, m q: discharge intensity, m^2/s H_1: fall height, m g: gravitational acceleration
(6)	[10]	$d_s = 1.5q^{0.6}H_1^{0.1}$	d_s: scour hole depth, m q: discharge intensity, m^2/s H_1: fall height, m
(8)	[11]	$d_s = 1.413q^{0.5}H_1^{0.25}$	d_s: scour hole depth, m q: discharge intensity, m^2/s H_1: fall height, m
(9)	[45]	$\frac{d_s}{d_w} = 3.13\left(\frac{q}{\sqrt{gd_w^3}}\right)^{0.867}\left(\frac{H_1}{R}\right)^{3.11}$	d_s: scour hole depth, m d_w: tail water depth, m R: radius of the bucket, m q: discharge intensity, m^2/s H_1: fall height, m
(10)	[2]	$\frac{d_s}{d_w} = 6.914\left(\left(\frac{q}{\sqrt{gd_w^3}}\right)^{0.694}\left(\frac{H_1}{d_w}\right)^{0.0815}\left(\frac{R}{d_w}\right)^{0.233}\left(\frac{d_{50}}{d_w}\right)^{0.196}\Phi^{0.196}\right)$	d_s: scour hole depth, m d_w: tail water depth, m R: radius of the bucket, m q: discharge intensity, m^2/s H_1: fall height, m Φ: flip bucket angle, rad

where ω is a normal vector, $\frac{1}{2}\|\omega\|^2$ is the regularization factor, C is the error penalty factor, b is a bias, ε is the error function, x_i is the input vector, d_i is the target value, l is the number of elements in the training data set, $\varphi(x_i)$ is a feature space, and ξ_i and ξ_i^* are upper and lower excess deviation. Table 4 provides a compilation of well-known kernel functions [35,36].

2.3. Overview of the GEP

The GEP is an extension of genetic programming and genetic algorithms, initially developed by Ref. [37]. In the GEP, the genome is encoded as linear chromosomes of fixed length, which are then translated into a phenotype represented as expression trees. Similar to other hybrid evolutionary techniques, the GEP algorithm commences with the random generation of an initial population comprising individual chromosomes of fixed length. The fitness of each chromosome is assessed through an evaluation function. The creation of new generations involves the application of genetic operators such as mutation, inversion, transposition, and recombination. Subsequent adjustments are made to the new individuals either until a specified maximum number of generations is reached or until the desired level of precision is attained. Within the GEP model, the primary objective is to generate a mathematical equation using training data. A visual representation of the GEP process is presented in Fig. 3.

2.4. Overview on the MARS

As a non-parametric regression analysis, the MARS has been formulated by Ref. [38] to achieve precise, flexible and quick regression outcomes. Describing and extracting a nonlinear relationship between independent and target variables is the main superiority of MARS. It bursts the datasets into numerous regions to match a regression model to each region. While knots are called the break values between regions, the term basis function is utilized to prove each district interval of the independent variables. The form of basic functions are as below:

$$\max(0, x - k) \text{ or } \max(0, k - x) \tag{16}$$

Where x denotes independent variable and k is a threshold value [39]. MARS common formulation form is as below:

$$y = f(x) + \varepsilon \tag{17}$$

$$f(x) = \beta_o + \beta_m BF_m(x) \tag{18}$$

which y stands for the target variable evaluated by the unknown function f(x), ε is the error, β_o is coefficient of the constant value, BFm is the m-th basis function and β_m is coefficient of BFm. The maximum number of BFs that is convenient for data is illustrated by m value in Eq. (18). The most fit node points are determined using generalized cross validation (GCV) index as below [38–41]:

$$GCV = \frac{1}{N}\left[\frac{\sum_{i=1}^{N}(y_i - f_M(x_i))^2 y_i - f_M(x_i))^2}{\left(1 - \frac{\overline{(C(M)}}{N}\right)^2}\right] \tag{19}$$

which N shows data number and $\overline{C}(M)$ refers a complexity penalty functions that can be presented by:

$$\overline{C}(M) = C(M) + d.M \tag{20}$$

where C(M) is the quantity of linearly independent BF, M refers the knots number decided in the forward process, and d is the penalty for every BF involved in the developed model [42].

2.5. Overview of the MLP

The MLP is a fundamental architecture of the ANN used in ML and AI. It is a type of feed forward neural network, meaning that information flows in one direction, from input to output, without feedback loops. The MLPs are composed of multiple layers of interconnected nodes or neurons, each layer consisting of one or more neurons. These neurons are organized into an input layer, one or more hidden layers, and an output layer.

In the MLP architecture, each neuron in a layer is connected to every neuron in the subsequent layer, and each connection has a weight associated with it. Neurons in the hidden layers and the output layer apply an activation function to the weighted sum of their inputs to produce an output. This allows MLPs to model complex non-linear relationships in data. Training an MLP involves adjusting the weights of its connections using techniques like back propagation and gradient

Table 2
A summary of literature review of DDMs application for scouring prediction.

References	Included DDMs	Outcomes
[16]	The SVR and the SVRwith algorithm of innovative gunner (SVR-AIG)	The SVR-AIG-based estimations are more accurate than the SVR standalone model estimations.
[17]	The BR, the ABR, the SVR	The ABR had the best outcomes among the other models
[18]	The GEP, the MARS, the M5P Tree, the RF, the RT, the REP-Tree	The GEP based model is more accurate than other prediction methods.
[17]	The DT, the ABR, the XGBoost, the LightGBM	All models have precise outcomes.
[19]	The MLP, the RBF, the RF, and the MARS	The MLP had superior performance.
[20]	The GBDT, the ET, the RF	The GBDT had the highest accuracy and lowest error.
[21]	The GBDT, the CFNN, the KRR	The GBDT model outperformed the CFNN and KRR.
[46]	The M5MT, the CART, the MARS	The MARS technique was the best approach for the estimation of scour depth.
[22]	The ANN, the ANFIS, the SVR optimized with Fruitfly Optimization Algorithm (SVR-FOA).	the proposed SVR-FOA method performed well
[23]	The HHO, the ANN, the ANN-HHO, the ANN-PSO, the ANN-GA	The accuracy of accuracy of the ANN-HHO was more than th others.
[24]	The ANFIS integrated with ptimization methods namely cultural algorithm, biogeography based optimization (BBO), invasive weed optimization (IWO) and teaching learning based optimization (TLBO)	the ANFIS-IWO can be used as a reliable and cost-effective method for predicting the scouring depth downstream of weirs.
[25]	The MARS, the ANN	The MARS technique was the superior one
[26]	The GEP, the MT, the evolutionary polynomial regression approaches	The MT approach yielded the most precise predictions in comparison with the other proposed models.
[27]	The SVM, the M5, the CART	The CART produces better prediction compared to other techniques.
[5]	The ANN, the GP	The GP based estimations were found to be equally and more accurate than the ANN based ones

Table 3
Observations of the prototype.

Number	q (m^2/s)	H_1 (m)	d_s(m)	Number	q (m^2/s)	H_1 (m)	d_s(m)	Number	q (m^2/s)	H_1 (m)	d_s(m)
1	34.2	31.72	12.19	39	69.5	92.35	17	77	79.26	47	29
2	25.1	20.29	8.08	40	39	49	27.4	78	116	64.92	35.96
3	72.49	30.42	18.29	41	47.6	26.6	24.7	79	79.06	154.2	8.82
4	42.76	46.18	19.51	42	143.43	19.45	16	80	52.95	97.53	36.88
5	21.37	12.55	19.51	43	48	90	70	81	79.33	98.45	48.76
6	3.62	24.85	10.37	44	78	88.5	88	82	57.5	122.8	27.43
7	75.8	85	28	45	26.5	96	23	83	32.6	102.1	13.41
8	113.6	180	43	46	53.1	97.8	37	84	7.67	24	5.53
9	68.8	49	20	47	79.6	98.5	49				
10	40	34	20	48	47.8	220	62				
11	25	31	19	49	96.5	32	35.4				
12	95.2	97	30	50	42.56	83.5	32				
13	2.6	1.8	2.5	51	25.86	83.5	32				
14	1.8	1.9	2.4	52	41	49	18				
15	17	6.3	14.3	53	41.2	83.5	32				
16	60	7.3	16.2	54	55.99	84	32				
17	32	26	11	55	48.98	83.5	41				
18	50	14	18	56	56.2	84	41				
19	14	9	6.4	57	61.33	83.5	41				
20	34	32	12.2	58	46.5	23	18				
21	25	27	8.1	59	97.54	47.85	15				
22	72	36	18.3	60	97.54	47.84	23				
23	43	50	19.5	61	42.6	56.7	19.5				
24	21	19	19.5	62	21.5	21.8	28.2				
25	3.6	25	10.4	63	46.5	25	10				
26	170	53	55	64	275	101	68				
27	60	17	17	65	57.58	163	27.5				
28	48	19	24	66	20.51	102	13.5				
29	70	19	32	67	31.4	27	15				
30	10	30	9	68	14	12	6.35				
31	32	6	11.5	69	96.3	148	37.5				
32	31.4	4	11	70	32.62	143	23				
33	25	8	16.5	71	12.1	97	12				
34	14	1	6.35	72	275	91	68				
35	83.3	115.44	47	73	26.5	96	23				
36	112.71	212.9	37.2	74	53.1	97.8	37				
37	39.3	115.74	10.6	75	79.6	98.5	49				
38	51.3	86.53	11.4	76	116.66	65	36				

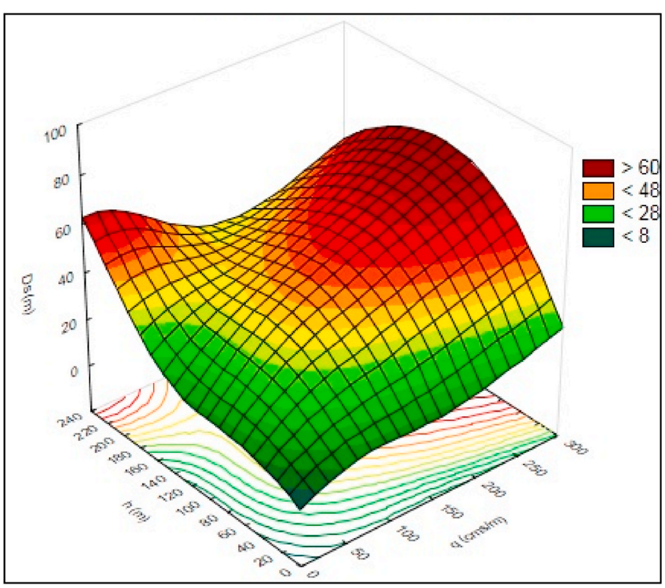

Fig. 2. A 3D view of ds variation against (H, q).

descent. This training process aims to minimize the difference between the network's predictions and the actual target values for a given dataset. MLPs are used for various machine learning tasks, including classification, regression, and pattern recognition. Fig. 4 illustrates a schematic depiction of the architecture of the MLP.

Table 4
Types of Kernel functions.

Kernel name	Function
Linear	$K(x_i, x_j) = (x_i, x_j)$
Polynomial	$K(x_i, x_j) = [(x_i, x_j) + 1]^d$
Redial Basis Function (RBF)	$K(x_i, x_j) = \exp\left[-\frac{\lVert x_i - x_j \rVert^2}{2\sigma^2}\right]$
Exponential Radial Basis Function (ERBF)	$K(x_i, x_j) = \tanh[-\alpha(x_i, x_j) + c]$

2.6. *Indices of performance assessment*

To evaluate the quality of model outcomes in comparison to the target values, the following indices were employed: Root Mean Square Error (RMSE), determination of coefficient (R^2), and mean average error (MAE):

$$RMSE = \sqrt{\frac{\sum_{i=1}^{N}(y_i - x_i)^2}{n}} \tag{21}$$

$$R^2 = \left[\frac{N\left(\sum_{i=1}^{N} x_i y_i\right) - \left(\sum_{i=1}^{N} x_i\right)\left(\sum_{i=1}^{N} y_i\right)}{\sqrt{\left[N\sum_{i=1}^{N} x_i^2 - \left(\sum_{i=1}^{N} x_i\right)\right]\left[N\sum_{i=1}^{N} y_i^2 - \left(\sum_{i=1}^{N} y_i\right)\right]}}\right]^2 \tag{22}$$

$$MAE = \frac{\sum_{i=1}^{N}|x_i - y_i|}{N} \tag{23}$$

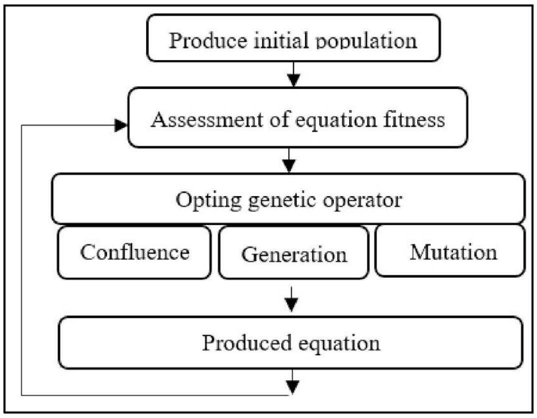

Fig. 3. Flowchart of the GEP algorithm.

Here y_i and x_i are target and predicted values of relative scour depth, respectively, $\overline{y}$ and $\overline{x}$ are mean values of target and predicted relative scour depth, respectively, and N is the total number of the dataset. It is worth noting that the aforementioned indices provide an average measure of predictive error values without conveying information about error distribution. In addition to these indices, a supplementary metric known as the Developed Discrepancy Ratio (DDR), introduced by Ref. [43]; has been incorporated as an additional assessment tool for evaluating model performance:

$$DDR = \frac{\text{Predicted Value}}{\text{Observed Value}} - 1 \tag{24}$$

An insightful visual representation of DDR, utilizing the standard normal distribution format derived from the Gaussian function of DDR values, provides a more discerning assessment of model performance. Normalized values of scour depth, Z_{DDR}, are calculated after standardizing the DDR values extracted from Gaussian function of the DDR, S_{DDR}. In a scatter plot depicting the graphical relationship between Z_{DDR} and S_{DDR}, it becomes evident that error distribution tendencies gravitate towards the centerline. Additionally, larger values of extreme S_{DDR} correspond to heightened levels of accuracy.

3. Results and discussion

3.1. Analysis of DDMs included

Complexity arises in DDMs, and their utility can be constrained due to the multitude of input parameters necessary to predict the target parameter. To address this challenge, this research strategically incorporates the Froude number, $Fr = \frac{q}{\sqrt{gH_1^3}}$, as readily calculable from hydraulic variables, as an independent input parameter for forecasting the target parameter $\left(\frac{d_s}{H_1}\right)$ in the models. The share of the allocated data into the training and the testing phases of DDMs were 70 % and 30 %, respectively. The performance evaluation metrics for the four data-driven models during both the training and testing phases are delineated in Table 5.

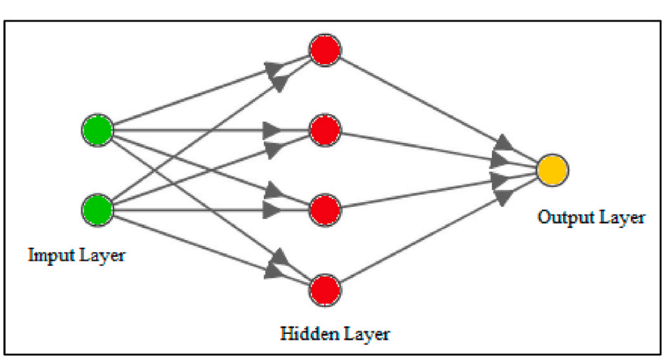

Fig. 4. General form of the MLP structure.

Table 5
Summary of statistical indices for DDMs outputs for testing phase.

		RMSE	MAE	R^2	DDR_{max}
Training phase	SVM	0.28754	0.19800	0.94180	1.693
	GEP	0.40928	0.25978	0.90488	1.229
	MLP	0.20613	0.11716	0.98100	2.767
	MARS	**0.08665**	**0.05714**	**0.99169**	**4.519**
Testing phase	SVM	0.0901	0.0648	0.9313	2.133
	GEP	0.1628	0.1200	0.7146	1.124
	MLP	0.0583	0.0478	0.9738	2.950
	MARS	**0.0252**	**0.0170**	**0.9933**	**9.144**

STATISTICA.12 software was used to perform the simulation using the SVM model. Two classification methods employed in the SVM include Nu-SVM and C-SVM, as described by Ref. [44]. In the former, C is established as a parameter utilizing the available noise information within the dataset. Conversely, in the latter method, the values of Nu serve as upper and lower error bounds for the support vectors. Following rigorous calculations, it was determined that the Nu-SVM model yielded the most favorable outcomes for classification. The Radial Basis Function (RBF) Kernel function was judiciously chosen as the most optimal for executing the model on the measured data, as determined through a systematic trial-and-error procedure. The parameter values were set as follows: $C = 8$, $Nu = 0.25$ and $\gamma = 11$. The values of the (RMSE, MAE, R^2) indices were obtained for both the training and the testing stages as follows: (0.28754, 0.1980, 0.9418) and (0.0901, 0.0648, 0.9313), respectively. These numerical results substantiate the correct execution of the model training process, as evidenced by the test phase exhibiting a notably higher relative accuracy. The execution of the GEP was carried out using the GeneXpro Tool 4.0 software. To derive the optimal formula, an extensive number of generations were generated and evaluated. The optimal formula was deduced employing operators including $+$, -, $\times$,/, exp(x), x^{-1}, x^2, and x^3 based on setting parameters outlined in Table 6. By cross-referencing Tables 5 and it is evident that the training phase of the Gene Expression Programming (GEP) model has been successfully executed, yielding the following performance metrics: RMSE $=$ 0.40928, MAE $=$ 0.25978, $R^2 = 0.90488$. Furthermore, the testing phase of the GEP model has been conducted, yielding the following performance metrics: RMSE $=$ 0.1628, MAE $=$ 0.1200, $R^2 =$ 0.7146. Fig. 5 provides a visual representation of the tree expression of the GEP model. The constants of the models are as follows: G1C0 $=$ 6.470001, G1C1 $=$ 8.091095, G2C0 $= -3.724213$, G2C1 $=$ 9.700867, G3C0 $=$ 1.063232, G3C1 $=$ 9.824585.

MATLAB software was used to run the MLP model to simulate scour depth. The selected MLP 1-5-1 model, as evidenced by the outcomes reported in Table 5, exhibited the following performance measures

Table 6
The values of the setting parameters in the GEP.

Parameters	Value
Head size	7
Chromosomes numbers	30
Number of genes	3
Mutation rate	0.09
Inversion rate	0.1
One-point recombination rate	0.3
Two-point recombination rate	0.3
Gene recombination rate	0.1
Gene transposition rate	0.1
IS transposition rate	0.1
RIS transposition rate	0.1
Fitness function error type	RMSE
Linking function	$+$

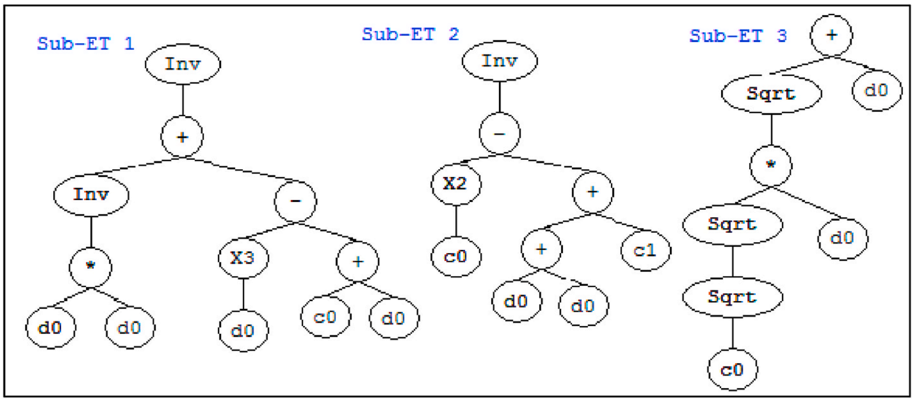

Fig. 5. Tree expression of GEP output.

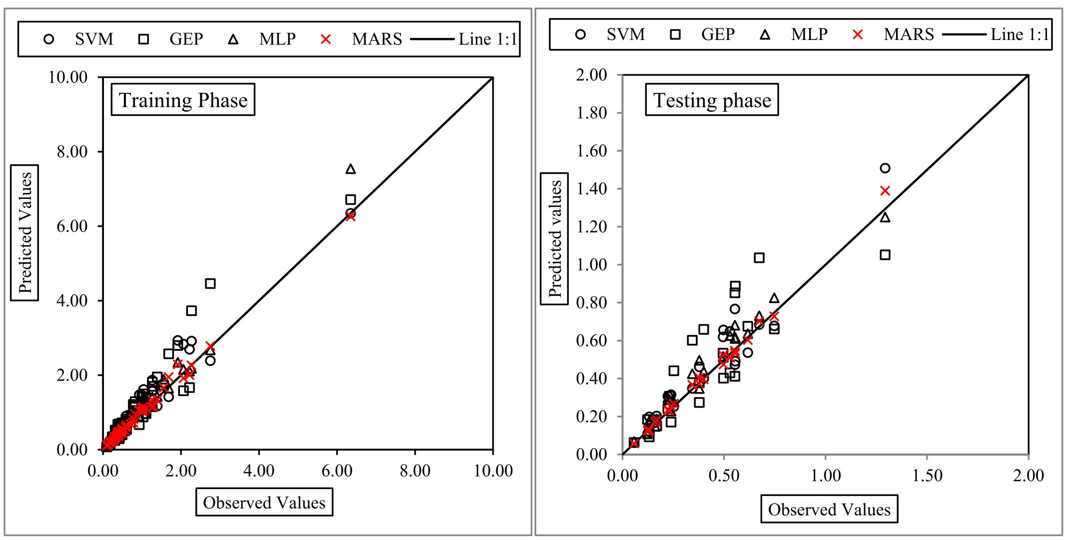

Fig. 6. Scatter plot of DDMs included's outcomes vs. observed data during the training and the testing phases.

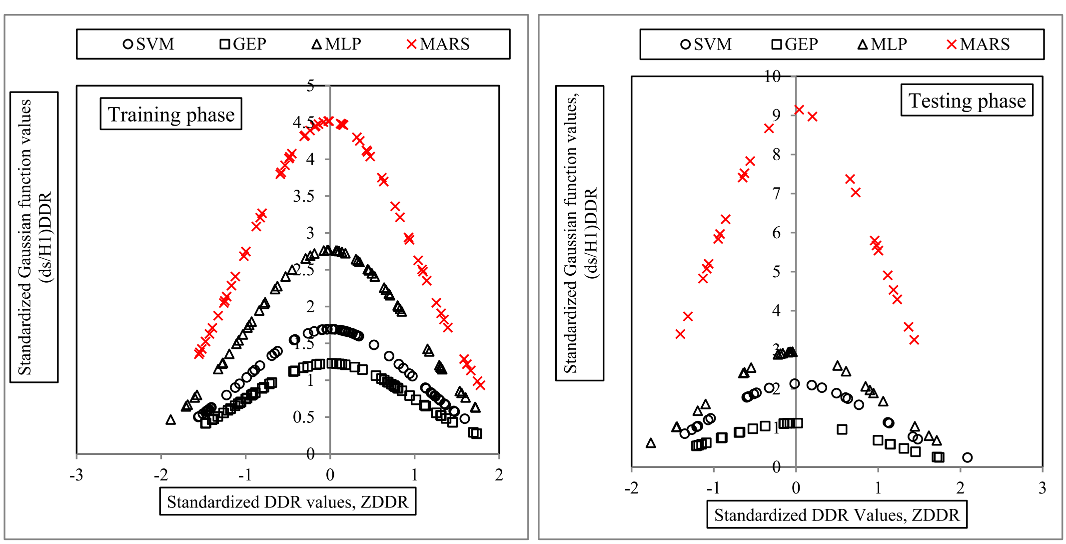

Fig. 7. Distribution of ZDDR for DDMs.

during the training phase: RMSE = 0.20613, MAE = 0.11716, and R^2 = 0.981. Likewise, during the testing phase, the model showcased the ensuing performance metrics: RMSE = 0.0583, MAE = 0.0478 and R^2 = 0.9738. Notably, it is worth highlighting that the model employed the Tanh activation function for the hidden layer and the Identity activation function for the output layer.

The MARS Model was applied to the collected data using STATISTICA.12 Software. The MARS model, representing the final and most

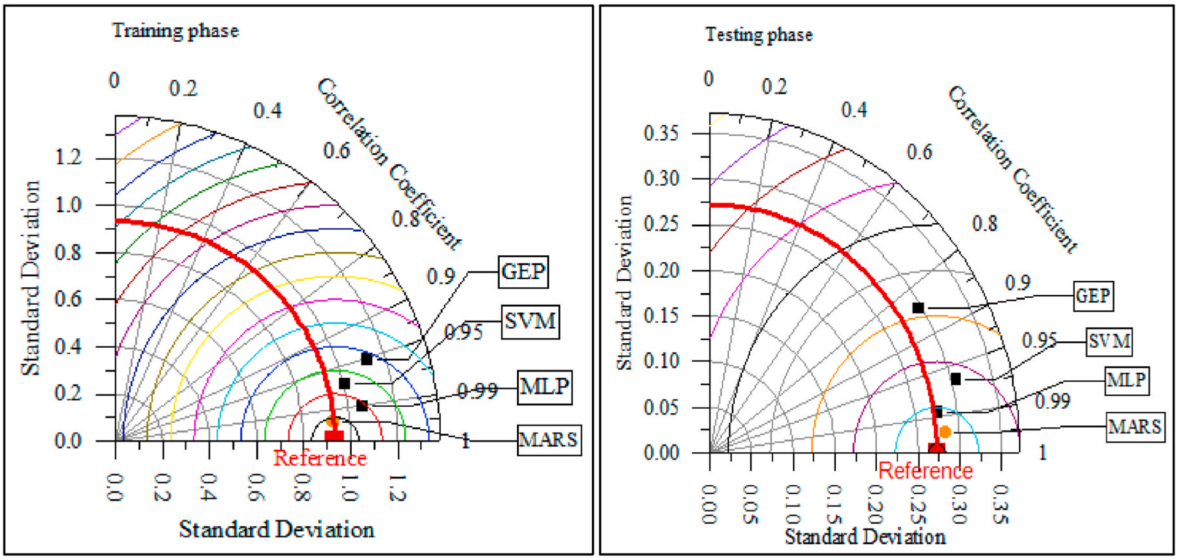

Fig. 8. Tylor diagram for DDMs for both the training and the testing stages.

Table 7
Summary of statistical indices of empirical relation included.

Developer	RMSE	MAE	R^2	DDR $_{max}$
[7]	0.57775	0.30908	0.59474	0.796
[8]	0.41348	0.24791	0.76465	0.836
[1]	**0.39667**	**0.17463**	**0.96172**	**1.428**
[10]	0.39559	0.22135	0.84948	1.038
[11]	1.06712	0.34295	0.88314	0.698

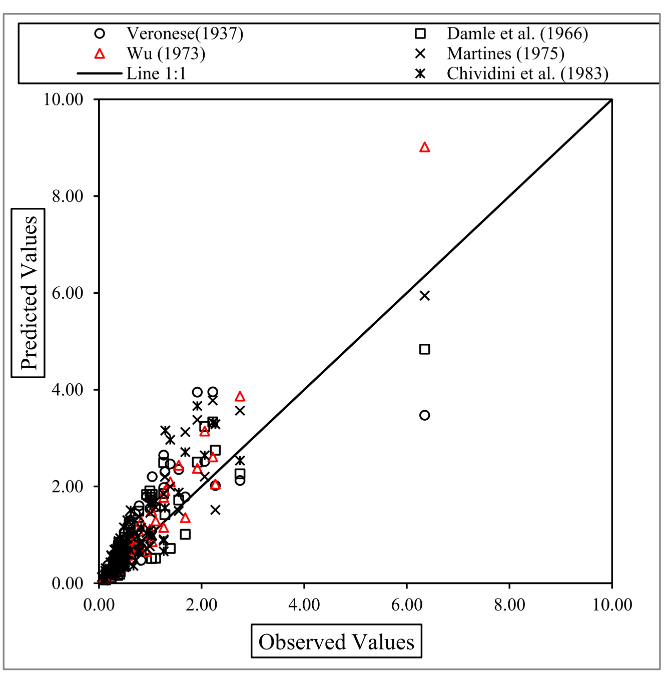

Fig. 9. Scatter plot view of the empirical equations performance.

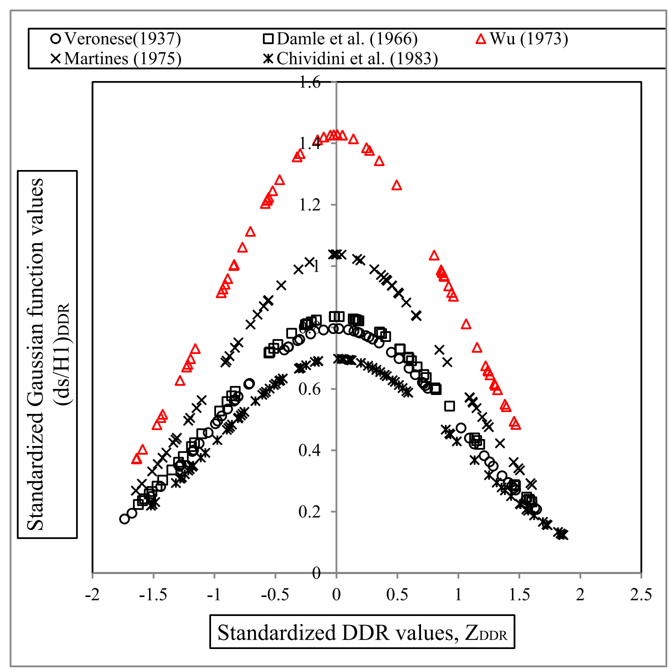

Fig. 10. Distribution of Z_{DDR} values for the empirical formulas.

optimal model among those considered, yielded the following performance evaluation metrics: during the training phase, the model achieved RMSE = 0.08665, MAE = 0.045714, R^2 = 0.99169, while during the testing phase, it delivered RMSE = 0.0252, MAE = 0.0170, R^2 = 0.9933. The values of model specifications including number of terms, number of basis function, order of interactions, penalty, threshold and GCV are 2, 1, 1, 2, 0.0005 and 0.12821, respectively. The following model should be used directly to forecast scour depth:

$$Ds = 0.00477 + 1.44855875148789 * \max(0, Fr - 0.0040438) \tag{25}$$

A scatter plot curve relative to the ideal 1:1 line represents an additional approach for assessing simulator performance. In this graphical representation, the narrower the distribution of data points around the ideal line, the greater the relative superiority of the corresponding simulator. Put differently, a smaller distance between the data points and the ideal line signifies the proximity of the simulator's behavior to that of the superior model. Fig. 6 presents a scatter plot of the four DDMs' outputs and target dataset. As depicted in the diagram, it is evident that the minimum and maximum distances from the ideal line are associated with the MARS and GEP models, respectively. However, it is essential to acknowledge that the distance from the ideal line tends to

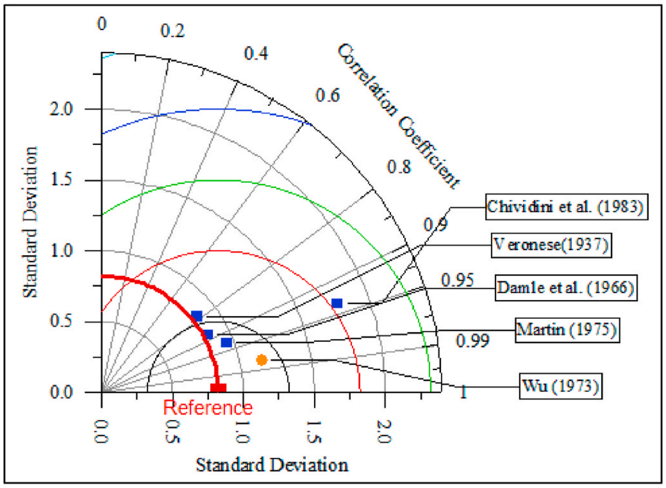

Fig. 11. Taylor diagram for empirical equations.

be more pronounced in the context of larger datasets.

Referencing the elucidations pertaining to the DDR index, Fig. 7 visualizes the performance of the DDMs as determined by the distribution of this index throughout both the training and testing stages. According to the insights derived from Fig. 7, the MARS emerges as the top-performing model, showcasing superior performance in both the training and test phases. Specifically, the MARS model exhibits the highest values of the $\left(\frac{d_s}{H_1}\right)_{DDR}$ parameter, amounting to 4.51 in the training phase and 9.14 in the testing phase. Consequently, upon analysis of the $\left(\frac{d_s}{H_1}\right)_{DDR}$ parameter, the MLP, the SVM and the GEP models are subsequently ranked as the second, third, and fourth best models, respectively. The Taylor diagram is a graphical representation that quantifies the alignment of model outputs in relation to reference points, employing statistical metrics such as the correlation coefficient and standard deviation. Smaller distances on the Taylor diagram signify higher levels of accuracy in the models' predictions. In accordance with the information provided, Fig. 8 showcases Taylor's diagram for the DDMs during both the training and testing phases. This figure unmistakably highlights the superior performance of the MARS model in comparison to the other three models.

3.2. Analysis of empirical equations

In accordance with the data presented in Table 1, a comparative evaluation was conducted on five commonly utilized empirical formulas, namely [1,7,8,10], and [11]. The values for the RMSE, MAE, R^2 and DDR indices pertaining to each of the equations are provided in Table 7.

The model proposed by Ref. [1] is identified as the superior model within this analysis. It exhibits the lowest RMSE and MAE indices and the highest R^2 and DDR_{max} indices. Conversely, the least accurate predictions are associated with the equations formulated by Refs. [7,11]. In order to assess the performance of each of the five experimental equations graphically, a scatter plot is depicted in Fig. 9, showing the predicted and observed dataset. The model with the shortest distance from the ideal 1:1 line on this curve will indicate its relative superiority. Clearly, in this figure, it is evident that the model proposed by Ref. [1] exhibits the least deviation from the ideal line.

The graphical comparison of the performance of five experimental models based on the DDR index, as depicted in Fig. 10, reveals that the [1] model stands out as the superior model among the others. This determination is supported by its observation of the highest peak and the narrowest distribution curve when compared to the vertical axis. The Taylor diagram, presented in Fig. 11, visually represents the disparity between predicted data and the reference data. This diagram unequivocally substantiates the superior performance of [1] model.

4. Conclusions

One of the primary objectives of spillway design is to effectively dissipate energy at high dams, thereby mitigating downstream scouring. This aspect of spillway design holds paramount importance for dam safety, as scouring downstream represents one of the most critical and potentially hazardous issues that can arise. In this study, DDMs are developed for the prediction of scouring depth downstream of the flip-bucket spillway. The novelty of the study lies in the use of field data and using readily Froude number parameter as input variable. The innovation presented in this research can be summarized in two significant aspects: (i) utilization of field-measured data: the research incorporates the novel approach of utilizing field-measured data, which adds a valuable real-world dimension to the study; (ii) simplification of DDMs: the research simplifies the complexity associated with DDMs by relying on a single readily input variable, namely the Froude number. This streamlines the modeling process and enhances its practical applicability. In the current paper, an exploration of the capabilities and potential of the SVM, the GEP, the MLP and the MARS has been undertaken. The objective is to predict the scour depth downstream of a flip-bucket spillway utilizing field-collected data. In addition to these DDMs, five empirical equations have also been employed. The findings of this investigation are as follows.

- All four DDMs exhibit acceptable potential for predicting scour depth. Nevertheless, the MARS model outperforms the other models in terms of all evaluation indicators, indicating its superior performance.
- Furthermore, when comparing the five regression equations using performance evaluation indices, the model proposed by Wu (1937) demonstrated relatively higher accuracy. However, in the direct comparison between the DDM and the regression model, the results unequivocally establish that the MARS model possesses a substantial and statistically significant advantage over the empirical equation.

Funding

This research did not receive any specific grant from funding agencies in the public, commercial, or not-for-profit sectors.

Author contribution

H. Md Azamathulla and Mehdi Fuladipanah conceived of the presented idea. Data curation was performed by H.Md Azamathulla. Methodology and software were done by Mehdi Fuladipanah, Kiran Tota-Maharaj and Vishwa nathdahm Mandala. Validation and visualization were conducted by H. Md. Azamathulla and Kiran Tota-Maharaj. Writing and original draft were provided by Mehdi Fuladiapanh and Aaron Chadee. Review and editing were performed by H. Md. Azamathulla.

Declaration of competing interest

The Authors of this paper declare that he has no conflict of interest.

Data availability

Data will be made available on request.

References

[1] C.M. Wu, Scour at downstream end of dams in Taiwan, in: International Symposium on River Mechanics, 1973, pp. 1–6. Bangkok, Thailand, Vol. I: A13.
[2] H Md Azamathulla, Neural Networks to Estimate Scour Downstream of Ski-Jump Bucket Spillway, Ph.D. Thesis, Indian Institute of Technology, Bombay, 2005.
[3] B. Achour, L. Amara, D. Mehta, Control of the hydraulic jump by a thin-crested sill in a rectangular channel-new experimental considerations, Larhyss J. (2022) 31–48.
[4] D.L. Strelchuk, Scour at the Base of Spillway Buckets, in: Electronic Theses and Dissertations, vol. 6840, University of Windsor, Windsor Ontario, Canada, 1969.
[5] H Md Azamathulla, A.A.B. Ghani, N.A. Zakaria, S.H. Lai, C.K. Chang, C.S. Leow, Z. Abuhasan, Genetic programming to predict ski-jump bucket spillway scour, J. Hydrodyn. 20 (4) (2008) 477–484.
[6] A. Schokiltsch, Prevention of Scour and Energy Dissipation, Translated at the USBR, USA, 1935.
[7] A. Veronese, Erosioni de Fondo a Valle di uno Scarico, Annali dei LavoriPublicci 75 (9) (1937) 717–726.
[8] P.M. Damle, C.P. Venkatraman, S.C. Desai, Evaluation of scour below ski-jump buckets of spillways, Proc. CWPRS Golden Jubilee Symp. Poona, India I (1966) 154–163.
[9] S.P. Chee, P.V. Padiyar, Erosion at the base of flip buckets, Canadian Engineering journal 52 (11) (1969) 22–24.
[10] R.B.F. Martines, Scouring of rocky river beds by free jet spillways, Int. Water Power Dam Constr. 27 (4) (1975) 152–153.
[11] M. Chividini, R.A. Lopardo, G.F. Vernet, C.M. Angelaccio, Maximum scour estimation downstream ski-jump spillways, Anales del XI Congreso Nacional del Agua, Córdoba, Argentina 6 (1983) 187–210.
[12] A. Najah Ahmad, A. El-Shafie, O.A. Karim, O. Jaafar, Integrated versus isolated scenario for prediction dissolved oxygen at progression of water quality monitoring stations, Hydrol. Earth Syst. Sci. 15 (2011) 2693–2708.
[13] A. Najah Ahmad, T.V. Lam, N.D. Hung, N.V. Thieu, O. Kisi, A. El-Shafie, A comprehensive comparison of recent developed meta-heuristic algorithms for streamflow time series forecasting problem, Appl. Soft Comput. 105 (2021), 107282.
[14] M. Rezaie-Balf, N. Fathollahzadeh Attar, A. Mohammadzadeh, M.A. Murti, A. Najah Ahmed, C.M. Fai, N. Nabipour, S. Alaghmand, A. El-Shafie, Physicochemical parameters data assimilation for efficient improvement of water quality index prediction: comparative assessment of a noise suppression hybridization approach, J. Clean. Prod. 21 (271) (2020), 122576.
[15] M. Ehteram, F. Binti Othman, Z. Mundher Yaseen, H. Abdulmohsin Afan, M. Falah Allawi, M. Bt Abdul Malek, A. Najah Ahmed, S.P. Shahid, V. Singh, A. El-Shafie, Improving the muskingum flood routing method using a hybrid of particle Swarm optimization and bat algorithm, Water 10 (2018) 807–829.
[16] L. Wang, G. Zhang, X. Yin, H. Zhang, M.H. Kashani, T. Roshni, S.G. Meshram, Hybrid model of support vector regression and innovative gunner optimization algorithm for estimating ski-jump spillway scour depth, Appl. Water Sci. 13 (1) (2023) 11.
[17] L. Kumar, M.S. Afzal, S. Ghosh, A novel-tuned Custom ensemble machine learning model to predict abutment scour depth in clear water conditions, AQUA-Water Infrastructure (2023).
[18] F. Salmasi, P. Sihag, J. Abraham, M. Nouri, Experimental investigation and prediction of free fall jet scouring using machine learning models, Int. J. Sediment Res. 38 (3) (2023) 405–420.
[19] R. Mirzaee, M. Mohammadi, S.F. Mousavi, M. Bagherzadeh, K. Hosseini, Application of soft computing techniques to estimate the scouring depth formed by crossing jets, Water Sci. Technol. 87 (8) (2023) 1853–1865.
[20] M. Rashki Ghaleh Nou, M. Azhdary Moghaddam, Prediction of scour depth downstream of the flip bucket with machine learning techniques, Proceedings of the Institution of Civil Engineers-Water Management 175 (4) (2022) 178–189 (Thomas Telford Ltd).
[21] M. Pandey, M. Jamei, I. Ahmadianfar, M. Karbasi, A.S. Lodhi, X. Chu, Assessment of scouring around spur dike in cohesive sediment mixtures: a comparative study on three rigorous machine learning models, J. Hydrol. 606 (2022), 127330.
[22] X. Sun, Y. Bi, H. Karami, S. Naini, S.S. Band, A. Mosavi, Hybrid model of support vector regression and fruitfly optimization algorithm for predicting ski-jump spillway scour geometry, Engineering Applications of Computational Fluid Mechanics 15 (1) (2021) 272–291.
[23] S.S. Sammen, M.A. Ghorbani, A. Malik, Y. Tikhamarine, M. AmirRahmani, N. Al-Ansari, K.W. Chau, Enhanced artificial neural network with Harris hawks optimization for predicting scour depth downstream of ski-jump spillway, Appl. Sci. 10 (15) (2020) 5160.
[24] A. Sharafati, M. Haghbin, S.B. Haji Seyed Asadollah, N.K. Tiwari, N. Al-Ansari, Z. M. Yaseen, Scouring Depth Assessment Downstream of Weirs Using Hybrid Intelligence Models. Applied Science, Advance online publication, 2020.
[25] M. Rezaie-Balf, Multivariate adaptive regression splines model for prediction of local scour depth downstream of an apron under 2D horizontal jets, Iranian Journal of Science and Technology, Transactions of Civil Engineering 43 (2019) 103–115.
[26] M. Najafzadeh, A. Tafarojnoruz, S.Y. Lim, Prediction of local scour depth downstream of sluice gates using data-driven models, ISH Journal of Hydraulic Engineering 23 (2) (2017) 195–202.
[27] M.K. Ayoubloo, H Md Azamathulla, Z. Ahmad, A.A. Ghani, J. Mahjoobi, A. Rasekh, Prediction of scour depth in downstream of ski-jump spillways using soft computing techniques, Int. J. Comput. Appl. 33 (1) (2011) 92–97.
[28] K.A. Zvorykin, T.K.H. Akhmedov, Scour of rock bed by a jet splitting from a deflecting bucket of an overflow dam, 16th IAHR, Sao Paulo, Brazil 2 (1975) 418–422.
[29] P. Sen, Spillway scour and design of plunge pool, Journal of Irrigation Power 41 (1) (1984) 51–66.
[30] T.K.H. Akhmedov, Calculation of the depth of scour in the rock downstream of a spillway, Int. Water Power Dam Constr. 40 (12) (1988) 25–27.
[31] R.M. Khatsuria, State of Art on Computation, Prediction and Analysis of Scour in Rocky Beds Downstream of Ski-Jump Spillways, CWPRS, Platinum Jubilee Symposium, Poona, India, 1992.
[32] D. Yildiz, E. Üzücek, Experience gained in Turkey on scours occurred downstream of the spillways of high dams and protective measurements, in: Proceeding of 18th ICOLD, 1994, pp. 113–135. Durban, Q. No. 71, R9.
[33] R.A. Lopardo, M.C. Lopardo, J.M. Casado, Local Rock Scour Downstream Large Dams, Proceeding of International Work shop on Rock scour due to high velocity jets, Lausanne, Switzerland, 2002, pp. 55–58.
[34] V. Vapnik, The Nature of Statistical Learning Theory, Springer-Verlag., New York, 1995, pp. 113–141.
[35] H Md Azamathulla, F.C. Wu, Support vector machine approach for longitudinal dispersion coefficients in natural streams, Appl. Soft Comput. 11 (2) (2011) 2902–2905.
[36] H Md Azamathulla, M.A.M. Yusoff, Z.A. Hasan, Scour below submerged skewed pipeline, J. Hydrol. 509 (2014) 615–620.
[37] C. Ferreira, Gene expression programming: a new adaptive algorithm for solving problems, Complex Syst. 13 (2) (2001) 87–129.
[38] J.H. Friedman, Multivariate adaptive regression splines, Ann. Stat. 19 (1991) 1–67.
[39] M. Zabihi, H.R. Pourghasemi, Z.S. Pourtaghi, M. Behzadfar, GIS-based multivariate adaptive regression spline and random forest models for groundwater potential mapping in Iran, Environ. Earth Sci. 75 (2016) 665–683.
[40] P. Samui, D.P. Kothari, A multivariate adaptive regression spline approach for prediction of maximum shear modulus and minimum damping ratio, Engl. J. 16 (2012) 69–78.
[41] A. Parsaie, A.H. Haghiabi, Improving modelling of discharge coefficient of triangular labyrinth lateral weirs using SVM, GMDH and MARS techniques, Irrigat. Drain. 66 (2017) 636–654.
[42] J. Antanasijević, V. Pocajt, D. Antanasijević, N. Trišović, K. Fodor-Csorba, Prediction of clearing temperatures of bent-core liquid crystals using decision trees and multivariate adaptive regression splines, Liq. Cryst. 43 (2016) 1028–1037.
[43] R. Noori, A. Khakpour, B. Omidvar, A. Farokhnia, Comparison of ANN and principal component analysis-multivariate linear regression models for predicting the river flow based on developed discrepancy ratio statistics, Expert Syst. Appl. 37 (2010) 5856–5862.
[44] R.E. Fan, P.H. Chen, C.J. Lin, Working set selection using second order information for training support vector machines, J. Mach. Learn. Res. 6 (2005) 1889–1918.
[45] M. Ghodasian, Maximum depth of scour downstream of flip bucket, in: Proceeding River Flow, 2002, pp. 1079–1081. Belgium.
[46] R. Shafagh Loron, M. Samadi, A. Shamsai, Predictive explicit expressions from data-driven models for estimation of scour depth below ski-jump bucket spillways, Water Supply 23 (1) (2023) 304–316.